GA–A27072

CONTRIBUTIONS OF ELECTRON CYCLOTRON WAVES TO PERFORMANCE IN ADVANCED REGIMES ON DIII-D

by
C.C. PETTY, M.E. AUSTIN, D.P. BRENNAN, K.H. BURRELL, J.C. DeBOO, E.J. DOYLE,
J.R. FERRON, A.M. GAROFALO, J.C. HILLESHEIM, C.T. HOLCOMB, C. HOLLAND,
A.W. HYATT, Y. IN, G.L. JACKSON, J. LOHR, P.A. POLITZER, R. PRATER,
H. REIMERDES, T.L. RHODES, L. SCHMITZ, S.P. SMITH, W.M. SOLOMON,
G.M. STAEBLER, R. TAKAHASHI, F. TURCO, A.D. TURNBULL, M.A. VAN ZEELAND,
G. WANG, A.E. WHITE, and L. ZENG

MAY 2011

GENERAL ATOMICS

DISCLAIMER

GA–A27072

CONTRIBUTIONS OF ELECTRON CYCLOTRON WAVES TO PERFORMANCE IN ADVANCED REGIMES ON DIII-D

by

C.C. PETTY, M.E. AUSTIN,* D.P. BRENNAN,† K.H. BURRELL, J.C. DeBOO, E.J. DOYLE,‡ J.R. FERRON, A.M. GAROFALO, J.C. HILLESHEIM,‡ C.T. HOLCOMB,¶ C. HOLLAND,† A.W. HYATT, Y. IN,§ G.L. JACKSON, J. LOHR, P.A. POLITZER, R. PRATER, H. REIMERDES,# T.L. RHODES,‡ L. SCHMITZ,‡ S.P. SMITH, W.M. SOLOMON,Δ G.M. STAEBLER, R. TAKAHASHI,¶ F. TURCO,° A.D. TURNBULL, M.A. VAN ZEELAND, G. WANG,‡ A.E. WHITE,∞ and L. ZENG‡

This is a preprint of a paper to be presented at the 19th Topical Conf. on Radio Frequency Power in Plasmas, June 1–3, 2011, Newport, Rhode Island, and to be published in the *Proceedings.*

*University of Texas at Austin, Austin, Texas.
†University of Tulsa, Tulsa, Okalahoma.
‡University of California-Los Angeles, Los Angeles, California
¶Lawrence Livermore National Laboratory, Livermore, California.
§FAR-TECH, Inc., San Diego, California.
#Association Euratom-Confederation Suisse, CRPP, Lausanne, Switzerland.
ΔPrinceton Plasma Physics Laboratory, Princeton, New Jersey.
°Oak Ridge Associated Universities, Oak Ridge, Tennessee.
∞Massachusetts Institute for Technology, Cambridge, Massachusetts.

Work supported by
the U.S. Department of Energy under DE-FC02-04ER54698, DE-FG03-97ER54415, DE-FG02-08ER54984, DE-AC52-07NA27344, DE-FG02-07ER54917, DE-FG02-06ER84442, DE-AC05-00OR22725, DE-AC02-09CH11466, DE-FG02-04ER54761, DE-AC05-00OR23100, and DE-FC02-99ER54512

GENERAL ATOMICS PROJECT 30200
MAY 2011

GENERAL ATOMICS

Contributions of Electron Cyclotron Waves to Performance in Advanced Regimes on DIII-D

C.C. Petty[a], M.E. Austin[b], D.P. Brennan[c], K.H. Burrell[a], J.C. DeBoo[a], E.J. Doyle[d], J.R. Ferron[a], A.M. Garofalo[a], J.C. Hillesheim[d], C.T. Holcomb[e], C. Holland[f], A.W. Hyatt[a], Y. In[g], G.L. Jackson[a], J. Lohr[a], T.C. Luce[a], M.A. Makowski[e], M. Murakami[h], M. Okabayashi[i], P.A. Politzer[a], R. Prater[a], H. Reimerdes[j], T.L. Rhodes[d], L. Schmitz[d], S.P. Smith[a], W.M. Solomon[i], G.M. Staebler[a], R. Takahashi[c], F. Turco[k], A.D. Turnbull[a], M.A. Van Zeeland[a], G. Wang[d], A.E. White[l] and L. Zeng[d]

[a]General Atomics, P.O. Box 85608, San Diego, California 92186-5608
[b]University of Texas at Austin, Austin, Texas
[c]University of Tulsa, Tulsa, Oklahoma
[d]University of California at Los Angeles, Los Angeles, California
[e]Lawrence Livermore National Laboratory, Livermore, California
[f]University of California at San Diego, San Diego, California
[g]Far-Tech, Inc., San Diego, California
[h]Oak Ridge National Laboratory, Oak Ridge, Tennessee
[i]Princeton Plasma Physics Laboratory, Princeton, New Jersey
[j]Columbia University, New York, New York
[k]Oak Ridge Institute for Science Education, Oak Ridge, Tennessee
[l]Massachusetts Institute of Technology, Cambridge, Massachusetts

Abstract. High-power electron cyclotron (EC) waves are used to increase performance in several Advanced Tokamak (AT) regimes on DIII-D where there is a simultaneous need for high noninductive current and high beta. In the Quiescent High-confinement mode (QH-mode), a direct measurement of the electron cyclotron current drive (ECCD) profile is made using modulation techniques, and a trapped electron mode (TEM) dominated regime with core $T_e > T_i$ is created. In the "high q_{min}" AT scenario, ECCD provides part of the off-axis noninductive current and helps to produce a tearing stable equilibrium. In the hybrid regime, strong central current drive from EC waves and other sources increases the noninductive current fraction to ≈100%. Surprisingly, the core safety factor remains above unity, meaning good alignment between the current drive profile and the desired plasma current profile is not necessary in this scenario.

Keywords: ECCD, noninductive current drive, transport, stability
PACS: 52.35.Ra, 52.50.Sw, 52.55.Fa, 52.55.Wq

INTRODUCTION

Electron cyclotron (EC) heating and current drive is an important and versatile tool for tailoring the current density and pressure profiles on DIII-D. While many different topical areas utilize EC waves on DIII-D, the high power gyrotron program plays a critical role in Advanced Tokamak (AT) regimes where there is a simultaneous need for high noninductive current and high beta [1]. Three AT scenarios that have used EC waves to increase performance are the Quiescent High-confinement mode (QH-mode), the large bootstrap current fraction "high $q_{\min}$" scenario, and the low $q_{\min}$ hybrid scenario. Here, $q_{\min}$ refers to the minimum value of the safety factor. Central EC heating in QH-mode allows the study of turbulence and transport in low collisionality plasmas with the electron temperature exceeding the ion temperature ($T_e > T_i$) in the core. In the "high $q_{\min}$" AT scenario, experiments have optimized the safety factor profile and EC current profile for stable operation with high bootstrap current fraction. While the low value of $q_{\min}$ (≈1.05) in hybrid discharges results in a modest bootstrap current fraction (50%), the high on-axis current drive efficiency fully makes up for this deficiency, allowing ≈100% noninductive operation to be achieved. To date, six gyrotrons operating at 110 GHz (2nd harmonic X-mode) have been installed at DIII-D, injecting more than 3 MW into the plasma.

ECCD AND ELECTRON TRANSPORT IN QH-MODE

QH-mode produces plasmas without edge localized modes (ELMs) at constant density and radiated power, good edge particle exhaust, and increased energy confinement due to the H-mode edge pedestal [2]. An edge electromagnetic mode, the edge harmonic oscillation (EHO), causes enhanced particle transport that places the edge parameters in the stable region for peeling-ballooning modes. Because QH-mode discharges have low collisionality and are free of low frequency MHD activity, they are ideal for studying the ECCD profile in an AT regime.

The ECCD profile can be found directly from the periodic response of the motional Stark effect (MSE) signals to a modulation of the EC power [3,4]. For the situation where the plasma flux surfaces are fixed in space, the Fourier transform of the poloidal flux diffusion equation yields an ordinary differential equation that relates the modulated ECCD source ($\tilde{J}_{EC}$) to the modulation in the poloidal magnetic flux ($\tilde{\psi}$),

$$\frac{\partial^2\tilde{\psi}}{\partial\rho^2} + \left[\frac{1}{\rho} + \frac{\partial}{\partial\rho}\ln\left(\hat{F}\hat{G}\hat{H}\right)\right]\frac{\partial\tilde{\psi}}{\partial\rho} - \frac{i}{\hat{D}}\tilde{\psi} = -\mu_0 R_0 \rho_b^2 \frac{\hat{F}}{\hat{G}}\left[\left\langle\tilde{J}_{EC}\right\rangle + \frac{\tilde{\eta}}{\eta}\left\langle J_{oh}\right\rangle\right] \quad , \qquad (1)$$

$$\hat{D} = \frac{\eta}{\mu_0 \rho_b^2 \omega}\frac{\hat{G}\hat{H}}{\hat{F}} \quad , \qquad (2)$$

where η is the plasma resistivity, ρ is the normalized toroidal flux coordinate, ρ_b is the effective boundary radius, J_{oh} is the ohmic current density, ω is the modulation frequency, and $\hat{F},\hat{G},\hat{H}$ are geometry factors defined in Ref. [5]. Using Eq. (1), the measured modulation in the MSE signals, $\tilde{B}_z = (1/R)\partial\tilde{\psi}/\partial R$, can be used to experimentally determine the modulated ECCD profile.

Several steps can be taken to improve the accuracy in determining the ECCD profile using Eq. (1). First, modulating all of the gyrotrons in phase will modulate η, as well as the bootstrap current, through a modulation of T_e. This complication may be avoided by using a push/pull setup where co- and counter-injecting gyrotrons at the same deposition location alternate during each cycle so that the total heating power is constant with time. Second, the MSE diagnostic actually measures B_z at fixed (R,z) coordinates rather than at fixed ρ; therefore, $\tilde{\psi}$ must be corrected for any oscillations in the plasma position. Finally, in the high frequency limit ($\hat{D} << 1$), only the last term on the left hand side of Eq. (1) needs to be retained.

The measured ECCD profile for slightly off-axis deposition is shown in Fig. 1 for 5 Hz modulation with alternating co/counter injection. Since J_{EC} found from Eq. (1) actually represents the 0-to-peak amplitude for the sinusoidal component, the magnitude needs to be multiplied by $\pi/2$ to yield the peak-to-peak swing in the ECCD for square wave modulation. While localized current drive on the high-field and low-field side of the magnetic axis is observed at the predicted location, the experimental ECCD profile is broader than the theoretical TORAY-GA profile [6], although the integrated currents agree. The ECCD profile broadening could be due to gyrotron steering misalignment or radial diffusion of the current carrying electrons.

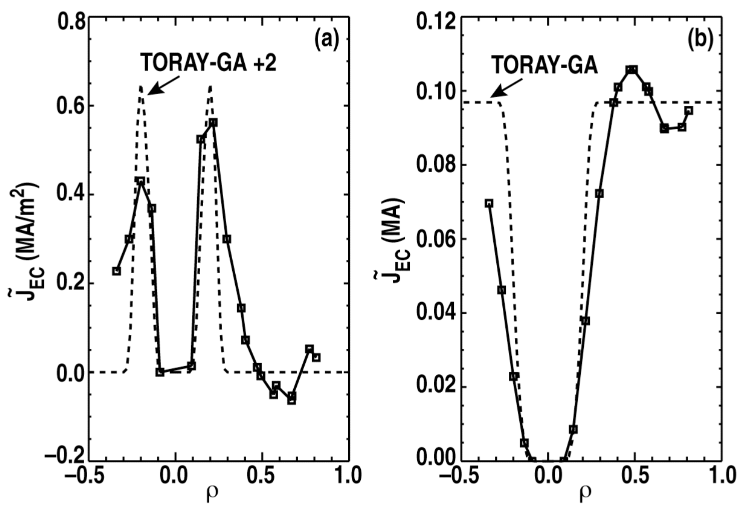

FIGURE 1. (a) Measured (solid curve) and theoretical (dash curve) flux-surface-average ECCD current density. (b) Measured (solid curve) and theoretical (dash curve) ECCD integrated current.

Understanding electron heat transport is important for developing low collisionality AT regimes with significant bootstrap current. Additionally, the electron channel will likely dominate transport in burning plasma experiments owing to strong electron heating from alpha particles. Electron transport is studied in QH-mode plasmas on DIII-D using 2.7 MW of central ECH, achieving $T_e(0) \approx 12$ keV and $T_e(0)/T_i(0) > 1$. The core collisionality is in the range expected for ITER ($\nu_e \sim 0.05$). During ECH, the central ion temperature and toroidal rotation are reduced; the lower rotation results in a lower $E \times B$ shear rate in most of the plasma. Only minor changes in the density profile are measured.

The measured fluctuations in the density and electron temperature, before and during ECH, are shown in Fig. 2 [7]. The density fluctuations at low and intermediate poloidal wavenumber, measured by Doppler Backscattering [8], are essentially unchanged by the strong central electron heating. However, since ECH increases $\rho_s = c_s m_i / eB_T$, where $c_s = \sqrt{kT_e / m_i}$, DBS actually measures different portions of the $k_\theta \rho_s$ spectrum before and during ECH. Taking into account other QH-mode data showing density fluctuation levels scaling inversely with $k_\theta \rho_s$, an increase in $\tilde{n}/n$ by at most 20%-30% during ECH can be inferred. In contrast, long wavelength ($k_\theta < 2\ \mathrm{cm}^{-1}$) T_e fluctuations measured by Correlation Electron Cyclotron Emission radiometry (CECE) [9] show a substantial increase with ECH. Increased T_e fluctuations are characteristic of Trapped Electron Mode (TEM) turbulence, as previously observed in DIII-D L-mode plasmas [10].

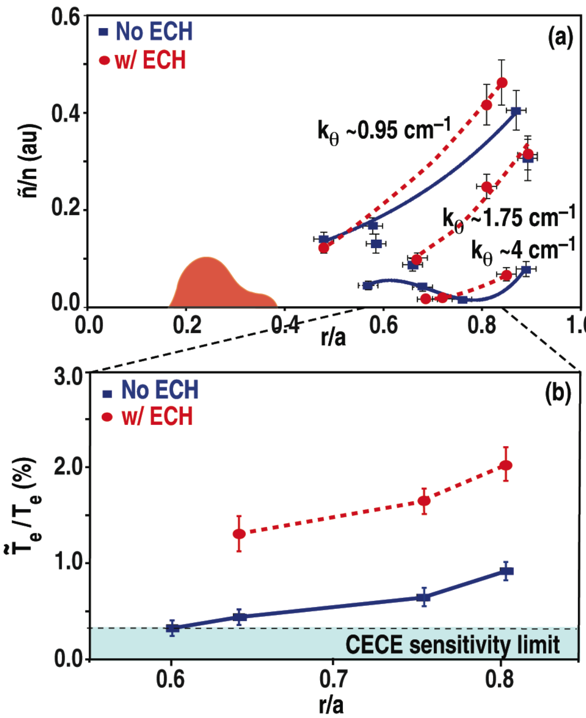

FIGURE 2. (a) Radial profiles of relative density fluctuation level before/during ECH for different poloidal turbulence wavenumbers as measured by DBS. (b) Electron temperature fluctuation level from CECE before/during ECH. The ECH profile and the ECE sensitivity limit are indicated.

Transport analysis finds that the electron and ion thermal diffusivities are increased during ECH for nearly all radii. The normalized electron temperature gradient, $R/L_{Te} = R\nabla T_e/T_e$, is close to the calculated TEM critical gradient both before and during ECH. Calculations of the linear growth rates using the Trapped Gyro-Landau-Fluid (TGLF) driftwave model [11] indicate a transition from a dominant Ion Temperature Gradient (ITG) mode to a dominant TEM with ECH. The TEM is enhanced because ECH increases T_e/T_i and reduces the normalized ion temperature gradient, $R/L_{Ti} = R\nabla T_i/T_i$. Interestingly, TGLF predicts no linearly unstable ion modes at low $k_\theta \rho_s$ during ECH. The transition to TEM-dominated with ECH is consistent with the higher electron thermal diffusivity and the substantial increase in electron temperature fluctuations. The increase in ion thermal diffusivity is due to a decrease in the $E \times B$ shear and a decrease in the calculated ITG critical gradient length, the latter due to the increase in T_e/T_i.

STABLE OPERATION IN "HIGH $q_{\min}$" SCENARIO

The goal of the "high $q_{\min}$" AT scenario is to achieve high bootstrap current fraction ($f_{BS} \geq 70\%$) without sacrificing fusion power density or fusion gain [1]. The bootstrap current fraction scales like $f_{BS} \propto q^2\beta$; thus, high β and high q (at all radii) are needed in this regime. In high f_{BS} discharges, the bootstrap current and safety factor profiles are nonlinearly coupled through the q dependence of transport [12]. Experiments on DIII-D have examined the effect of the J_{EC} configuration on stability and studied the alignment between J_{EC} and total current density at high f_{BS}.

A broad ECCD profile is found to help avoid tearing modes that limit the duration of an AT scenario with $q_{\min} > 2$, as shown in Fig. 3. In these discharges, β_N and the gyrotron power are kept fixed, but the location and width of the ECCD profile are varied. Cases with narrow ECCD profile at either $\rho = 0.4$ or $\rho = 0.55$ terminate early with a large *m*/*n*=2/1 tearing mode. On the other hand, the case with broad ECCD remains stable for the entire discharge. When the gyrotrons are turned off prematurely for broad ECCD cases, a *m*/*n*=2/1 tearing mode appears shortly afterwards.

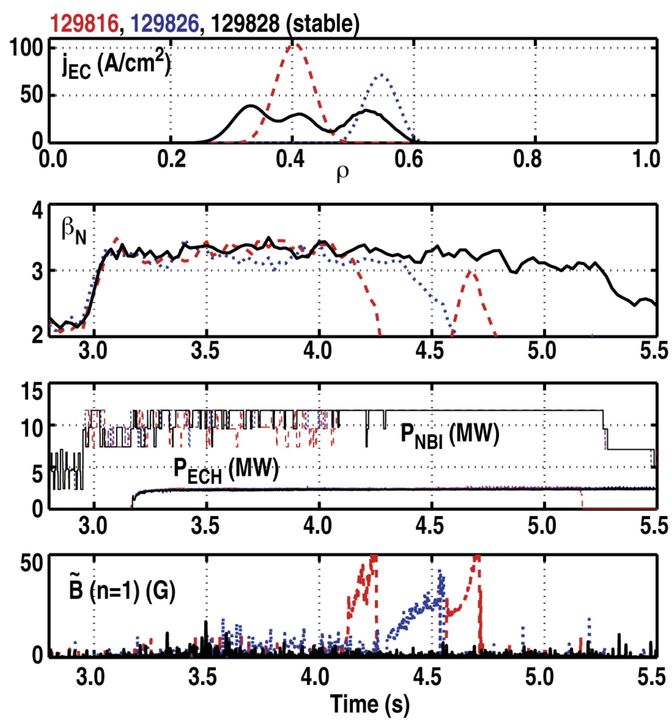

FIGURE 3. Comparison of MHD stability for the narrow and broad ECCD profiles. (a) EC current density. (b) Normalized beta. (c) NB and EC power. (d) rms amplitude of n=1 mode.

Scans to determine the best location for the broad ECCD profile do not yield a systematic result as both stable and unstable discharges are produced. Discharges free of tearing modes can be obtained with the ECCD center between $\rho = 0.45$ and $\rho = 0.6$, and with low EC driven current. However, discharges with similar ECCD profiles can be unstable to *m*/*n*=2/1 and *m*/*n*=3/1 tearing modes. An explanation for the variability of the results is the sensitivity of the tearing stability when close to the ideal "with wall" n=1 stability limit, which is confirmed by resistive stability calculations. Using the PEST3 code [13] and an experimental equilibrium, the ideal stability limit is approached by increasing the pressure or increasing the plasma-wall separation. PEST3 calculates that the classical tearing index Δ' increases sharply at the ideal stability boundary.

With on-axis neutral beams and off-axis EC sources, the highest f_{BS} is obtained at $q_{95} \sim 6.5$, and the best current alignment is at $q_{\min} \geq 1.5$. The plasma profiles are observed to broaden with increasing β_N and $q_{\min}$. With higher β_N, the bootstrap current increases and its profile broadens (owing to the broadening of the plasma profiles) which impacts the alignment with the total plasma current. The bootstrap current also increases with higher q_{95}, but interestingly the bootstrap current does not increase with higher $q_{\min}$. This is because the transport dependence on $q_{\min}$ offsets the favorable f_{BS} scaling with that parameter [12]. For high noninductive current cases ($f_{BS} \approx 80\%$) with $q_{95} = 6.8$, the shape of the noninductive current profile (using the broad, off-axis ECCD profile that is good for tearing mode stability) best matches the shape of the total current profile at $q_{\min} \geq 1.5$.

HIGH-BETA, STEADY-STATE HYBRIDS

A new AT regime with $q_{\min} \approx 1$ based on the hybrid scenario has been demonstrated on DIII-D. In principle, having $q_{\min} \approx 1$ should result in lower f_{BS} compared to the $q_{\min} > 2$ AT regime (although the difference in f_{BS} actually may be small owing to transport effects [12]), but this is offset by the higher current drive efficiency in hybrids since the required external current can be driven in the plasma center. These experiments show that the beneficial characteristics of hybrids, namely high stability limits and excellent confinement, are maintained when strong central current drive is applied to increase the noninductive current fraction to ≈100%.

Using central ECCD and neutral beam current drive (NBCD), high-beta hybrid discharges have approached steady-state conditions, as seen in Fig. 4. At $I_P = 1.08$ MA and $B_T = 1.9$ T, the heating and current drive power are ramped up until β_N reaches 3.4 and the surface loop voltage drops to 0.009 V. The measured loop voltage profile is small but positive at all radii. The achieved beta substantially exceeds the ideal "no-wall" n=1 stability limit calculated by DCON [14], with $C_\beta = (\beta - \beta_{\text{no-wall}})/(\beta_{\text{wall}} - \beta_{\text{no-wall}}) = 61\%$. The discharge has a small (4 G) m/n=3/2 tearing mode that plays an important role in broadening the current profile, discussed later. Despite the strong core electron heating that produces $T_e \approx T_i$ over the outer 80% of the minor radius, a high confinement factor of $H_{98y2} = 1.4$ is achieved. The resulting fusion performance factor $\beta_N H_{98y2}/q_{95}^2 = 0.14$ is sufficient for $Q = 5$ on ITER.

The calculated current drive is consistent with ≈100% noninductive current in this high-beta hybrid. The total ECCD from the CQL3D Fokker-Planck code is 0.17 MA, which includes a 30% quasi-linear enhancement of the current drive efficiency over the linear TORAY-GA value. The small loop voltage yields no appreciable synergy between the EC waves and the parallel electric field. The NBCD and bootstrap currents from TRANSP are 0.36 MA and 0.54 MA; thus, $I_{NI} = 1.07$ MA compared to $I_P = 1.08$ MA. For this central deposition, the current drive efficiency for ECCD is 0.055 A/W and for NBCD is 0.031 A/W; the bootstrap current fraction is 50%.

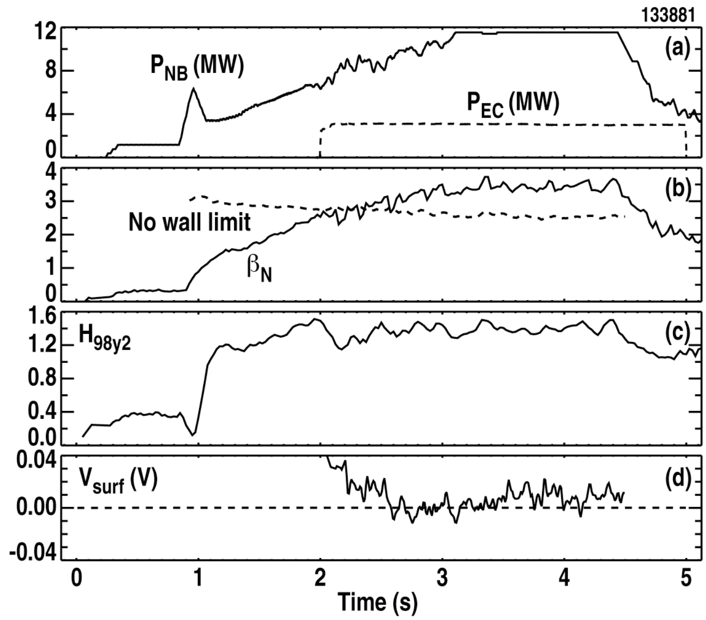

FIGURE 4. Hybrid discharge with ≈100% noninductive current drive. (a) NB and EC power. (b) Normalized beta and ideal no-wall limit. (c) IPB98(y,2) confinement factor. (d) Surface loop voltage.

Despite the strong central current drive, the sawtooth instability is mitigated and $q_{\min}$ remains around 1.1 in these hybrids. Figure 5(a) shows that the sum of the noninductive current densities is substantially more peaked than the total current density determined by equilibrium reconstruction including MSE data and the experimental pressure gradient. The effective inductive current density, the difference between the total and noninductive current densities, is plotted in Fig. 5(b). The negative core value is inconsistent with the measured (small) positive loop voltage profile. Therefore, the properties of the current profile are not in accordance with Ohm's law and neoclassical resistivity. The non-classical current density in Fig. 5(b) effectively (and anomalously) broadens the current profile, which is a standard feature of hybrid discharges with a *m/n*=3/2 tearing mode. Therefore, the poloidal magnetic flux pumping that occurs in inductively-driven hybrids [15] appears to also occur in noninductively driven hybrids. This is fortuitous as good alignment between the current drive profile and the desired plasma current profile is not necessary since the poloidal magnetic flux pumping in hybrids self-organizes the current density profile.

SUMMARY AND ACKNOWLEDGMENTS

High power EC waves have made many contributions to the AT regime on DIII-D. In QH-mode, central ECH simulates the condition of strong electron heating from alpha particles in burning plasma devices, causing the dominant turbulence mode to transition from ITG to TEM. This is observed experimentally in the larger electron temperature fluctuations and increased electron heat transport. This transition is a consequence of reduced R/L_{Ti} and increased T_e/T_i. In the 'high $q_{\min}$' AT regime, ECCD is used to provide part of the off-axis noninductive current, as well as to produce an equilibrium stable to tearing modes. With on-axis neutral beams and off-axis EC sources, the highest bootstrap current fraction is obtained at $q_{95} \sim 6.5$ and the best current alignment is at $q_{\min} \geq 1.5$. As a low $q_{\min}$ alternative, the hybrid scenario is shown to be compatible with high-performance, steady-state operation using central ECCD and NBCD. An advantage of the hybrid scenario is that it is not sensitive to alignment of the noninductive current profile and the total plasma current profile, but it may have lower ideal "with-wall" stability limits owing to its lower $q_{\min}$ operation.

This work supported by the U.S. DOE under DE-FC02-04ER54698, DE-FG03-97ER54415, DE-FG02-08ER54984, DE-AC52-07NA27344, DE-FG02-07ER54917, DE-FG02-06ER84442, DE-AC05-00OR22725, DE-AC02-09CH11466, DE-FG02-04ER54761, DE-AC05-00OR23100, and DE-FC02-99ER54512.

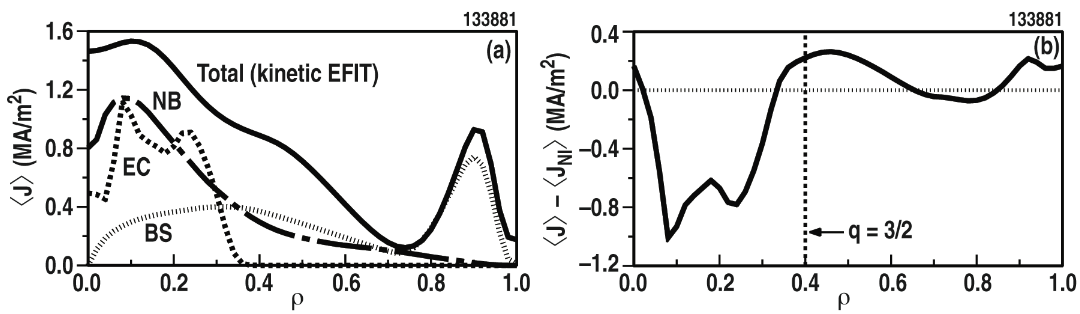

FIGURE 5. (a) Total current density from equilibrium reconstruction, and the modeled EC, neutral beam and bootstrap current densities. (b) Different between total and noninductive current densities, which is mainly the "non-classical" current density that broadens the hybrid current profile.

REFERENCES

1. T.S. Taylor, Plasma Phys. Control. Fusion **39**, B47 (1997).
2. K.H. Burrell et al., Phys. Plasmas **8**, 2153 (2001).
3. C.C. Petty et al., *Electron Cyclotron Emission and Electron Cyclotron Heating* (Proc. 13th Joint Workshop, 2004), Nizhny Novgorod: Russian Academy of Sciences, 2005, pp. 189-198.
4. C.C. Petty et al., "Modulated Current Drive Measurements" in *Radio Frequency Power in Plasmas*, edited by S.J. Wukitch and P.T. Bonoli, AIP Conference Proceedings 787, American Institute of Physics, Melville, NY, 2005, pp. 265-268.
5. H.E. St. John et al., *Plasma Physics and Controlled Nuclear Fusion Research* (Proc. 15th Int. Conf., Seville, 1994), Vienna: IAEA, 1996, vol. 3, pp. 603-606.
6. K. Matsuda, IEEE Trans. Plasma Sci. **17**, 6 (1989).
7. L. Schmitz at al., "Reduced Electron Thermal Transport in Low Collisionality H-mode Plasmas in DIII-D and the Importance of TEM/ETG-scale Turbulence" to be submitted to Nucl. Fusion.
8. J. Hillesheim et al., Rev. Sci. Instrum. **80**, 083507 (2009).
9. A.E. White et al., Rev. Sci. Instrum. **79**, 103505 (2008).
10. A.E. White et al., Phys. Plasmas **17**, 020701 (2010).
11. G.M. Staebler, J.E. Kinsey and R.E. Waltz, Phys. Plasmas **14**, 055909 (2007).
12. J.R. Ferron et al., Nucl. Fusion **51**, 063026 (2011).
13. A. Pletzer et al., J. Comput. Physics **115**, 530 (1994).
14. A. Glasser and M.S. Chance, Am. Phys. Soc. **42**, 1848 (1997).
15. C.C. Petty et al., Phys. Rev. Lett. **102**, 045005 (2009).